



Photoanodic oxidation of InP in acid solution and its surface chemistry: On the interplay of photons, protons and hydrodynamics

Dennis H. van Dorp^{a,*}, Genis Vanheusden^b, Kris Paulussen^{a,b}, Ibrahim Hassan^{a,b,c}, Simon Van Wonterghem^b, Graniel H. Abrenica^{a,b}, Praveen Dara^a, Johan Meersschaut^a, Thierry Conard^a, Frank Holsteyns^a, John J. Kelly^c

^a Imec, Kapeldreef 75, B-3001 Leuven, Belgium

^b Department of Chemistry, Katholieke Universiteit Leuven, Celestijnenlaan 200F, Leuven, B-3001, Belgium

^c Condensed Matter and Interfaces, Debye Institute for NanoMaterials Science, Utrecht University, Princetonplein 1, 3584 CC Utrecht, the Netherlands

ARTICLE INFO

Article history:

Received 15 May 2020

Revised 30 July 2020

Accepted 31 July 2020

Available online 5 August 2020

Keywords:

InP

GaAs

Anodic oxidation

Passivation

Native oxide

Surface chemistry

ABSTRACT

Factors determining etching and passivation of n-type InP in H₂SO₄ and HCl solution and the corresponding surface chemistry are considered. Passivation is favoured by higher light intensity and lower proton and Cl⁻ ion concentration. Ex-situ surface analysis shows the passive (bi)layer to consist mainly of oxide-based In³⁺ and P⁵⁺ components: InPO₄ and In(PO₃)₃. Hydrodynamics is found to play a decisive and surprising role in determining the kinetics of the surface reactions. Oxygen-bridge formation between surface In and P atoms, as a result of deprotonation of a P-OH reaction intermediate, is considered to be important in determining competition between the two reaction paths: etching and passivation. These results are compared with markedly contrasting results for n-type GaAs under similar experimental conditions.

© 2020 Elsevier Ltd. All rights reserved.

1. Introduction

Exciting developments in device technology have resulted in an upsurge of interest in III-V compound semiconductors such as InP and GaAs. These comprise improved fabrication techniques of nanowire/pillar arrays for photoelectrochemical energy conversion [1,2], phototransistors [3], flexible electronic devices [4,5], epitaxial integration on Si-based platform wafers enabling high volume manufacturing of CMOS transistors [6–9] and fully integrated photonic ICs, including laser and amplifier devices [10–14]. Various aspects of these technologies rely on high-quality etching of the semiconductor and an adequate understanding of the surface chemistry involved in the process. The ever-decreasing size of device structures requires ultimately atomic-layer-scale control of surfaces in terms of etching selectivity, stoichiometry and morphology [15,16].

In recent work we reported on the nanoscale wet-chemical etching of InP and GaAs in acidic solutions containing H₂O₂ as oxidizing agent [17]. The results indicate that the nature of the surface oxide determines a striking difference in the etching kinetics of the

two semiconductors. While GaAs shows a high chemical reactivity, the etch rate of InP is much lower, due to the formation of a thin stoichiometric passivating oxide. On the other hand, a strongly non-stoichiometric porous (hydr)oxide is formed on GaAs. We consider the critical factor governing the surface chemistry, and thus the etching properties, to be the ease with which an oxygen bridge can be formed between the group III and group V atoms when the surface bond is broken.

The marked contrast observed in the results of chemical etching of InP and GaAs has led us to reconsider electrochemical etching of the two semiconductors. Anodic oxidation of GaAs and its applications have received wide attention [18–21]. Fundamental studies of anodic oxidation of InP are fewer [22–24]. The electrochemical approach has been used successfully for (nano)porous etching of InP [25–29] and for studies of oxide growth [30–34]. In this paper we describe the results of a study of photoanodic oxidation and dissolution of n-type InP and, for comparison, n-type GaAs in H₂SO₄ and HCl solution. The basic electrochemistry was investigated by cyclic voltammetry and potential-step measurements. Surface analysis techniques (XPS, ToF-ERDA) provided useful information on the nature of the surface oxides. The important role of hydrodynamics was studied by using a rotating disk electrode and by cyclic voltammetry at variable potential-scan rate. The results reveal an interesting interplay of the experimental variables (pho-

* Corresponding author.

E-mail address: Dennis.vanDorp@imec.be (D.H. van Dorp).

ton flux, pH, Cl⁻ ion concentration and, in particular, hydrodynamics) that determines the mechanism and kinetics of anodic oxidation of InP. These results are contrasted with the markedly different results obtained with GaAs, and possible mechanisms of etching and passivation are discussed. Finally, trends observed in the two forms of etching, chemical and electrochemical, are compared.

2. Experimental

InP and GaAs (2 inch) substrates were obtained from AXT Inc. The n-type wafers had a (100) orientation and a carrier concentration in the range of 5–10E+16 cm⁻³. The dopant density of the p-type InP (111)-B wafers was 3–7E+17 cm⁻³. Chemicals were purchased from Sigma Aldrich and were of p.a. quality: 37% HCl (12.0 M), 96% H₂SO₄ (18.0 M) and 30% H₂O₂ (9.7 M). Prior to first use, wafers were cleaned in 1 M HCl/0.25 M H₂O₂ (InP) and 0.01 M HCl/0.005 M H₂O₂ (GaAs) for 5 min followed by ultra-pure water rinsing. All experiments were conducted in a cleanroom environment under controlled temperature (22 ± 1 °C) and relative humidity (40 ± 10%).

Ohmic contacts were provided on the n-type samples by depositing Ni/Au (100/200 nm) on the unpolished back side, followed by rapid thermal annealing (RTA) at 340°C for 20 min in a N₂-controlled chamber. For the p-type samples an Au:Zn/Au layer was used instead. Prior to metal deposition, the native oxide was removed by immersing the sample in 2 M HCl for 5 min followed by N₂ drying.

Electrochemical measurements were performed in a conventional three-electrode cell with a platinum counter electrode and saturated calomel electrode (SCE) as a reference. All potentials are reported with respect to SCE. Samples were mounted as a rotating disk electrode (RDE). The sample holder was equipped with a Kalrez O-ring to prevent leakage of electrolyte solution and to define a geometric area of 0.95 cm². The measurements were conducted at room temperature using a potentiostat (Princeton Applied Research, PARSTAT 4000) computer-controlled by VersaStudio software. Unless otherwise stated, the current-density potential (j-U) plots were recorded at a constant scan rate of 10 mV/s from negative to positive potential and back. The n-type electrodes were illuminated using a 150 Watt cold light source (Schott KL 1500). The light intensity was varied with neutral density filters (Edmund Optics). The maximum light intensity (100%) was in all experiments chosen to give an arbitrary limiting photocurrent density of approximately 6 mA/cm² under oxide-free conditions. When surface passivation was indicated by the j-U scan, the electrode was cleaned after each scan in 2 M HCl to prevent memory effects. A low HCl concentration was chosen to avoid the risk of chemical etching of InP by HCl [20]. A short H₂O rinse was subsequently applied. For each j-U plot, a minimum of three single potential scans were recorded to ensure reproducibility. For the potential-step experiments, the electrode was illuminated prior to and during the measurement.

Dissolution valence was determined by measuring the total charge by chronoamperometry and the etched volume by optical profilometry (WYKO NT3300).

Surface composition was studied by XPS. After etching, samples were rinsed for 30 s in ultra-pure water containing ~50 ppb of dissolved O₂. After N₂ blow-drying, the samples were transported in an N₂ atmosphere to the XPS set-up. The total "air exposure" was kept to less than 10 min. The measurements were carried out in Angle Resolved mode using a Theta300 system from Thermo Instruments. 16 spectra were recorded at exit angles between 22 and 78°, as measured from the normal of the sample. The integrated spectra shown in the figures are the summed intensities of 16 spectra measured at angles from 21 to 78°, allowing for higher in-

tensity peaks and hence more confidence in the fitting parameters. A monochromatized Al K α X-ray source (1486.6 eV) was used with a spot size of 400 μ m. The XPS core-level spectra were fitted with Avantage software using Smart background correction, the same relative constraints for elements and oxides and fixed FWHM fitting parameters were used. Standard sensitivity factors were used to convert peak areas to atomic concentrations.

Time-of-flight elastic recoil detection analysis (ToF-ERDA) was used for oxygen quantification. After etching, the samples were N₂ blow-dried and transported and loaded within 10 min in the experimental vacuum setup. ToF-ERDA measurements were performed at imec using a GSDH tandem accelerator with a maximum terminal voltage of 2.0 MV from National Electrostatics Corporation, Middleton (WI), U.S.A [35]. The impinging ion beam was either 8 MeV ³⁵Cl⁴⁺ or 10 MeV ⁶³Cu⁵⁺ used for these measurements. The respective incidence angle of the beam was 20° and 14.7° from grazing incidence with the ToF detector scattering angle at 40°. The signal from recoil oxygen is well separated in the spectrum and easily measured. Either the signal from ³⁵Cl⁴⁺ ions scattered on the heavy element (In) or the signal from recoiled phosphorus ions was used to determine the incident ion fluence. Integrated yield of the oxygen signal from the spectra and estimated ion fluence were used to quantify the areal densities of oxygen.

3. Results

Most of the experiments in this study were performed with n-type InP and GaAs under supra-bandgap illumination. This allowed us to regulate easily the density of active charge carriers (valence band holes). Three experimental approaches were used. Cyclic voltammetry revealed the general features of the kinetics of photoanodic etching of n-type InP in HCl and H₂SO₄ solutions. These results indicated the importance of a blocking layer that was studied with ex-situ surface analysis techniques (XPS and ToF-ERDA). The important role of hydrodynamics in determining the kinetics of oxidation was investigated with an InP rotating disk electrode (RDE) in potentiodynamic and potential-step experiments and in experiments in which the potential scan rate of a stationary electrode was varied. These results for InP are contrasted with results of cyclic voltammetric measurements performed on n-type GaAs under similar experimental conditions. In addition, for comparison some experiments were carried out with unilluminated p-type InP in H₂SO₄ solution.

3.1. Cyclic voltammetry

The photocurrent-potential characteristics of a stationary n-type InP electrode, measured in 1 M HCl solution, are shown in Fig. 1(a) for a range of relative light intensities (0–100%). Simple band-energy diagrams relevant for the different potential ranges are indicated in the figure. At negative potential, corresponding to weak band bending at the surface, photogenerated charge carriers (valence band holes) recombine with majority carriers (conduction band electrons), either directly or via bandgap states in the bulk and at the interface. As a result, no photocurrent is observed (range I). As the potential is made more positive, band bending at the interface increases, leading to spatial separation of electrons and holes. The electric field of the space-charge layer drives holes to the solid/solution interface where they cause oxidation and dissolution of the semiconductor. This results in an anodic photocurrent in the external circuit (range II). Recombination decreases until finally, at more positive potential, all photogenerated holes take part in the surface reaction and the photocurrent becomes independent of applied potential (range III). This limiting photocurrent j_L is directly proportional to the light intensity ϕ (see Fig. 1c). These re-

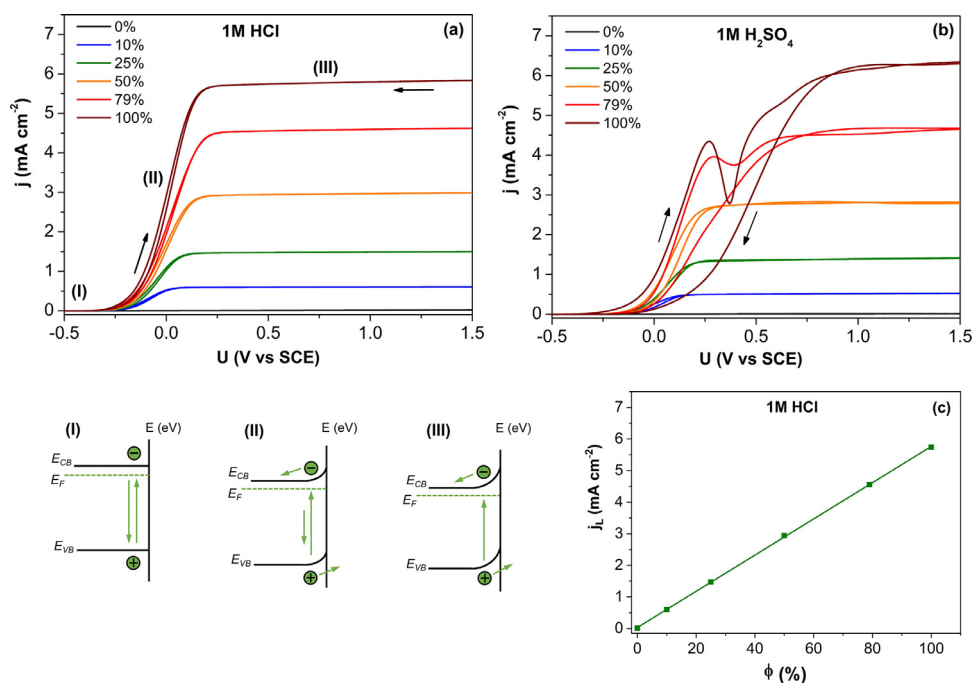
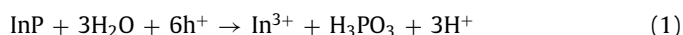


Fig. 1. Current density-potential (j - U) plots for a stationary n-type InP electrode illuminated at various relative light intensities (Φ) in (a) 1 M HCl and (b) 1 M H₂SO₄ solution. Fig. 1(c) shows the limiting plateau photocurrent j_L for 1 M HCl as a function of Φ . Schematic band-energy diagrams for the three relevant anodic regions are indicated in the figure.

sults are similar to those found for n-type GaAs in 1 M HCl solution (Fig. 2(a)).

From the literature it is known that six elementary charge carriers are required for anodic dissolution of one formula-unit of InP in acidic solution [20,22,36,37], the same also holds for GaAs [19–21,35], GaSb [38] and GaP[39]. We confirmed this result for n-type InP in 1 M HCl by determining the volume of the semiconductor dissolved for a given charge passed at 0.0 V (in the rising part of the photocurrent-potential curve) and at +1.0 V (in the limiting photocurrent range). In both cases we found that 6.0 ± 0.1 holes are indeed required to dissolve one formula-unit of the semiconductor. The oxidation reaction can be described by



The reaction products are the In³⁺ cation and phosphorous acid (H₃PO₃ i.e., P(OH)₃). In solution the latter converts to a more stable diprotic form of the acid, HPO(OH)₂ [40]. In 1 M HCl the In³⁺ cation will likely be complexed by chloride ions [41,42].

At low values of the photon flux, electron injection into the conduction band from intermediates of the anodic reaction may increase the quantum efficiency from 1 to 2 (three photons, instead of six, are required to dissolve one formula unit of InP) [36]. This might be the case for the lowest light intensities used in the present work, a point that will be considered in the discussion session.

Fig. 1(b) shows that the nature of the acid is important in determining the surface chemistry of InP. For 1 M H₂SO₄ solution at a relative light intensity of 50% and lower, the photocurrent-potential curve is similar to that measured for 1 M HCl at the same light intensity. For the 2 higher light intensities (79% and 100%) the expected limiting current is again reached at positive potential. However, a peak appears in the forward scan. The peak is more pro-

nounced at the higher light intensity (100%). In both cases a clear hysteresis is observed in the return scan to negative potential, in contrast to the results for 1 M HCl. The hysteresis is stronger for the higher light intensity. This result for H₂SO₄ suggests the formation of a surface layer. In contrast, the voltammogram measured with GaAs in 1 M H₂SO₄ at the highest light intensity was found to be the same as that for 1 M HCl and the limiting photocurrent was directly proportional to light intensity (Fig. 2(b)).

The “ideal” photocurrent potential curves shown in Fig. 1(a) for InP in 1 M HCl are no longer observed when the acid concentration is decreased to 0.1 M. For the higher light intensities of Fig. 3(a) (100%, 50%), complex voltammograms are found, consisting of two distinct peaks in the forward scan and strong hysteresis in the return scan. For the lowest light intensity shown (10%) there is a broad range in which the photocurrent is essentially independent of potential; this is the limiting value expected for the light intensity used. The voltammogram in this case shows some hysteresis, but only in the onset of photocurrent.

For 0.1 M H₂SO₄ at higher light intensity (25% and 100%) (Fig. 3(b)) the voltammograms show peak features similar to those of Fig. 3a, for 0.1 M HCl. The hysteresis in the return scan is more pronounced than is the case for 0.1 M HCl. The maximum current in both peaks is a factor of 2 or more higher for HCl than for H₂SO₄. In the latter case a lower light intensity of 5% is required to ensure a limiting, i.e. potential-independent, photocurrent with no hysteresis. In contrast to this InP result, the voltammogram for n-GaAs in 0.1 M H₂SO₄ solution at the highest light intensity (100%) shows features similar to those observed with InP and GaAs in 1 M HCl solution. The limiting photocurrent is linearly dependent on light intensity (see insert Fig. 2(b)). This also holds for a 0.1 and 0.01 M H₂SO₄ solution. Clearly, current-inhibiting layer formation is not a problem in the case of GaAs even at low proton concentration. Clear differences between results for InP in HCl and H₂SO₄ solutions were also observed at the intermediate acid concentra-

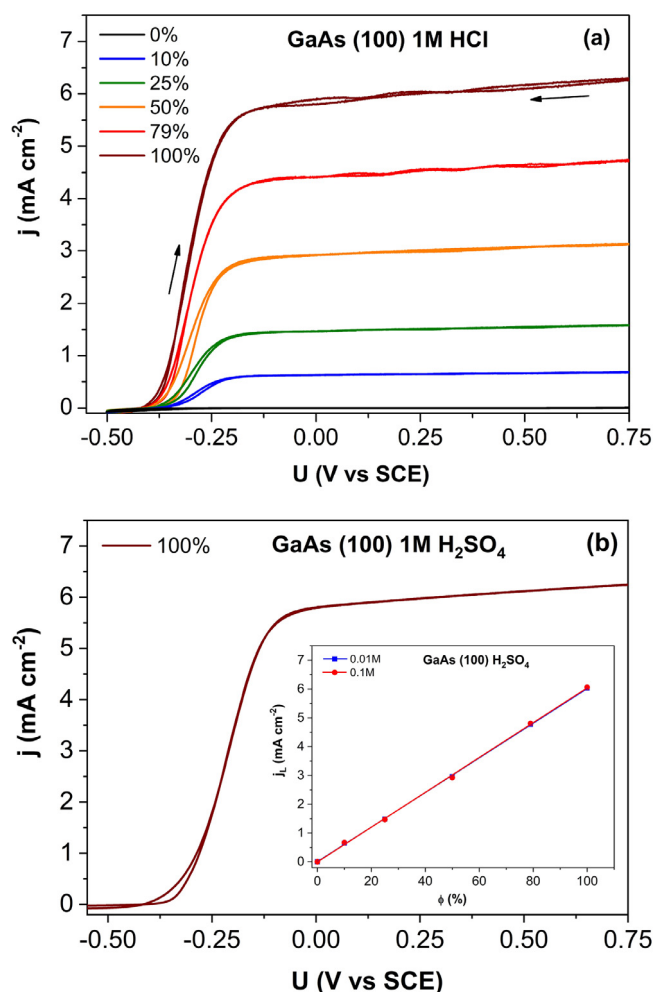


Fig. 2. Current density-potential plots recorded for a stationary n-type GaAs electrode at various light intensities in 1 M HCl solution (a). The plot measured for 1 M H₂SO₄ at 100% light intensity is shown in (b). The limiting photocurrent ($U = 0.5$ V) for 0.1 M and 0.01 M H₂SO₄, plotted as a function of light intensity, is shown in the insert.

tion of 0.25 M (supplement, Figure S1a). While the HCl result resembles with slight deviation that of 1.0 M HCl (Fig. 1(a)), the result for 0.25 M H₂SO₄ (Figure S1b) approaches that of 0.1 M H₂SO₄ (Fig. 3(b)) though with considerably higher current density.

Fig. 4(a) and 4(b) show that trends described for InP in 0.1 M HCl and H₂SO₄ solutions also hold when the acid concentration is reduced to 0.05 M, or lower. It is clear that, in the range down to 0.01 M, differences observed for the two acids are less pronounced than that at higher acid concentration. Here we note again that even at the highest light intensity (100%) and the lowest H₂SO₄ concentration (0.01 M) the expected limiting photocurrent density is observed for GaAs.

The general features of the cyclic voltammogram of n-type InP under illumination at lower acid concentration are also observed with p-type InP in the dark. This is shown in Figure S2 for a p-type (111)-B electrode in 0.05 M H₂SO₄ solution. As in the case of n-type, two peaks are observed in the forward scan and strong hysteresis in the return scan to negative potential. We note that for n-type InP the general electrochemical features as described above were not influenced significantly by the crystallographic orientation of the electrode surface.

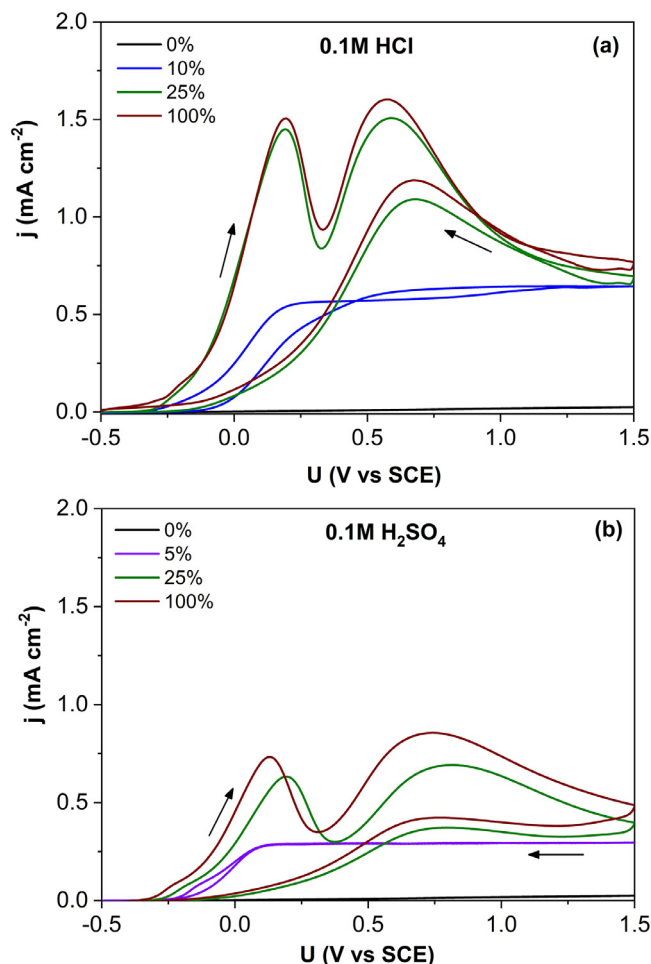


Fig. 3. Influence of light intensity on the current density-potential plot for a stationary n-type InP electrode recorded in (a) 0.1 M HCl and (b) 0.1 M H₂SO₄ solution.

3.2. Surface analysis

Two *ex-situ* techniques, XPS and ToF-ERDA, were used to investigate layer formation on n- and p-type InP at low acid concentration. The results reveal a relatively complex chemistry. To help understand the anodic oxidation mechanism, we examined the surface chemistry involved in the two distinct current-peak features by *ex situ* XPS for 0.05 M HCl and 0.05 M H₂SO₄ solution. Reference core-level P 2p and In 3d_{5/2} spectra for the HCl cleaned surface, i.e. prior to anodic oxidation, are shown in Fig. 5(a,b). (For a synchrotron XPS study of HCl-treated InP surfaces we refer to previous work [43,44].) The P 2p spectrum was fitted with 2 components: a P–In substrate peak and a small phosphorous oxide peak with a 4.5 eV chemical shift in binding energy with respect to the P–In substrate peak. It is clear that the surface was essentially free of either P³⁺ or P⁵⁺ related species [45]. The In 3d_{5/2} spectrum was more complex to fit as a result of the small chemical shift of In–O with respect to the In–P substrate peak. However, a small contribution from In³⁺ could be detected (see also reference [43]).

The P 2p and In 3d_{5/2} spectra for the first anodic peak are shown in Fig. 5(c, d) for 0.05 M HCl. The potential was scanned at full light intensity from –0.5 V to +0.37 V. The broad and pronounced higher binding energy feature in the P 2p spectrum indicates that the oxide consisted mainly of P⁵⁺ components. Previous work on anodic oxide formation in non-acidic electrolytes

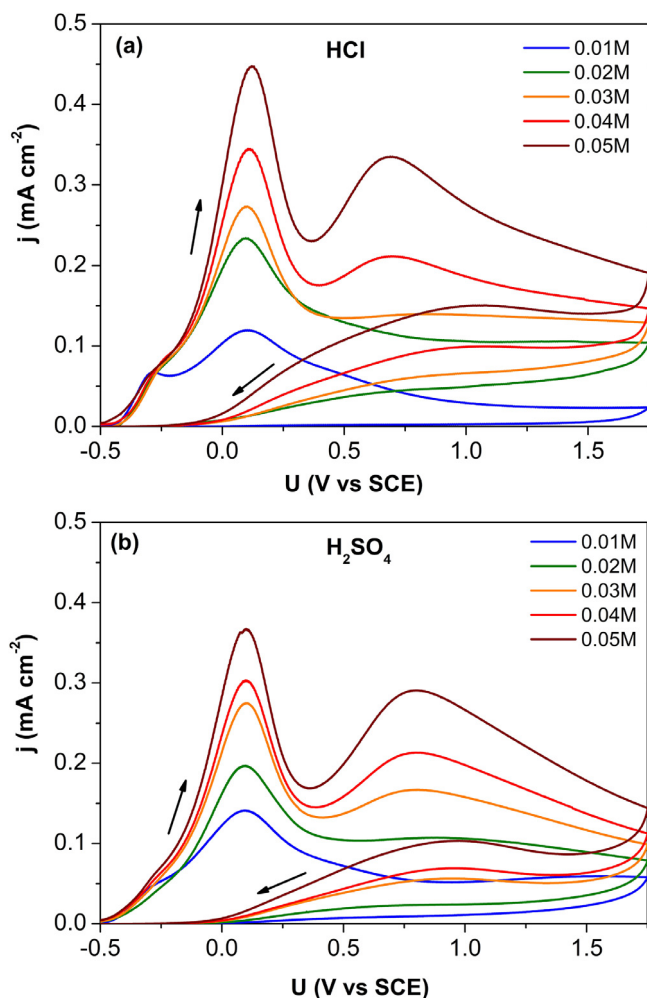


Fig. 4. Current density-potential plots for n-type InP for different acid concentrations in HCl (a) and H₂SO₄ solution (b). The maximum light intensity was used.

suggests that these components can most likely be attributed to stoichiometric InPO₄ (133.6 eV) and to the amorphous condensed phosphate In(PO_y)_x, with possibly some additional P₂O₅ at similar energy (134.6 eV) [30–34,46–48]. The smaller spectral weight of the lowest binding energy oxide component (132.7 eV) points to polyphosphate In(PO₃)₃. Finally, small amounts of elemental phosphorous (P⁰) were also detected. Similar results were found for the 0.05 M H₂SO₄ case (Figure S3 (a)). The In 3d_{5/2} spectra were deconvoluted into three components, with the main contributing peak positioned at 445.3 eV. These are attributed mainly to InPO₄, with some In(PO₃)₃ at similar binding energy, and In(PO_y)_x at higher energy. Due to the relatively large contribution in the In-P bulk range as compared to that of the P-In in the P 2p spectrum, it seems likely that In₂O₃ is also present in the oxide. However, it was not possible to resolve this peak as the associated binding energy is very close to the In-P substrate peak energy [49].

Spectral features for the second anodic peak, following a scan from -0.5 V to +1.75 V, are displayed in Fig. 5(e, f) for 0.05 M HCl. The absence of the P 2p_{1/2} and P 2p_{3/2} doublet peaks shows that the anodic oxide continued to grow during the course of the potential scan. The trend was supported by the O 1s core-level spectra that showed a peak intensity that was clearly higher for the second anodic peak (see also Figure S4). Also, in this case the oxide was mainly composed of the P⁵⁺ species: InPO₄, In(PO_y)_x/P₂O₅ and In(PO₃)₃. The spectral weight of In(PO₃)₃ was higher after scanning through the second anodic peak. The oxide features for the In 3d_{5/2} spectra were in good agreement with a main InPO₄/In(PO₃)₃ peak and a smaller In(PO_y)_x contribution. In₂O₃ was detected in low quantities. The H₂SO₄ experiment, however, showed lower amounts of P⁰ and In₂O₃ (Figure S3 (c, d)).

The atomic concentrations, as calculated from the fitted data, allowed us to determine the relative oxide composition P_{ox}/In_{ox} (P_{ox} and In_{ox} are the total oxide concentrations) as well as the relative contribution of the various oxide components. An overview of these results is summarized in Table 1. Oxide species related to the P 2p spectra were more abundant, while the fraction of In_{ox} was consistently lower. An acid dependence was not evident. The P 2p results for the two anodic peaks show that the oxide was

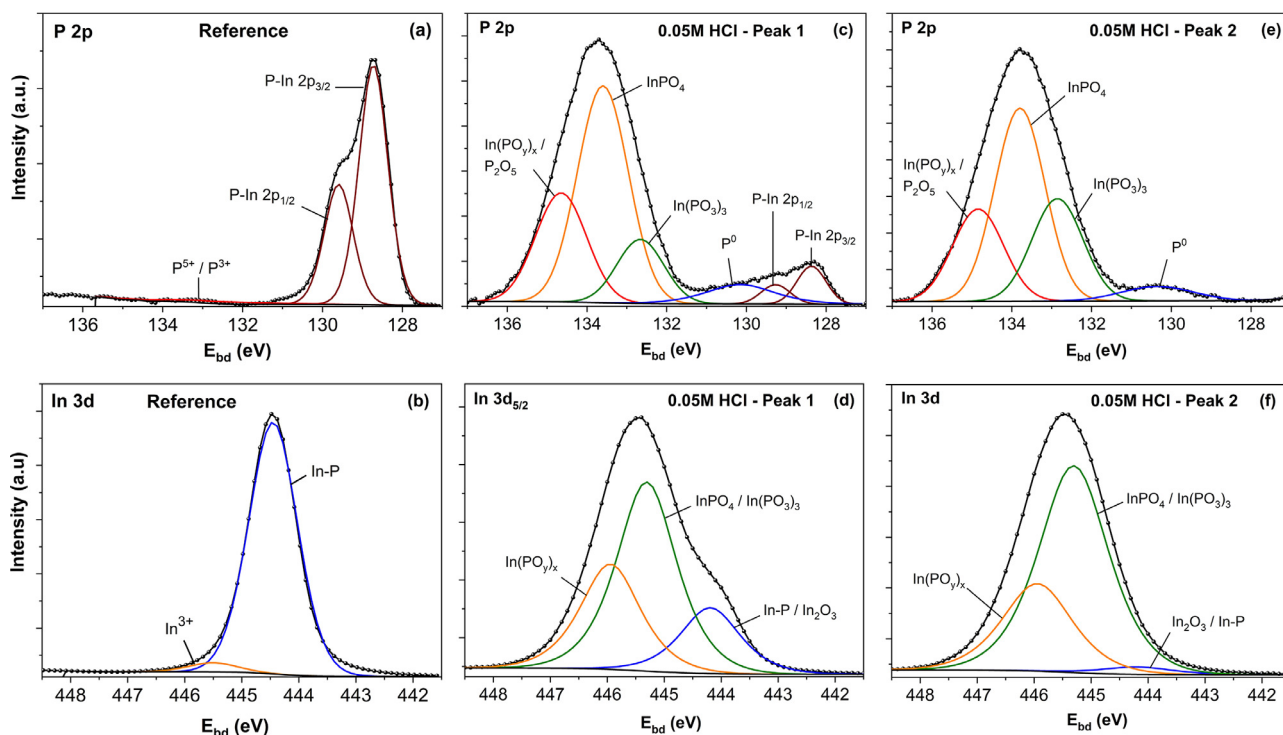


Fig. 5. Angle-integrated XPS spectra showing the P 2p and In 3d_{5/2} peak features obtained for the reference sample cleaned in 2 M HCl solution (a, b), after a potential scan through the first anodic peak (c, d) and the second anodic peak (e, f) in 0.05 M HCl solution. The final potentials were $U = 0.37$ V and $U = 1.75$ V, respectively.

Table 1

	HCl (peak 1)	H ₂ SO ₄ (Peak 1)	HCl (Peak 2)	H ₂ SO ₄ (Peak 2)
P_{ox}/In_{ox}	3.94	4.21	3.72	3.66
$InPO_4/P_{ox}$	0.56	0.58	0.49	0.46
$In(PO_3)_3/P_{ox}$	0.15	0.18	0.27	0.32
$In(PO_y)_x/P_{ox}$	0.28	0.25	0.24	0.22
$InPO_4/In_{ox}$	0.64	0.65	0.70	0.56
$In(PO_y)_x/In_{ox}$	0.36	0.35	0.30	0.44

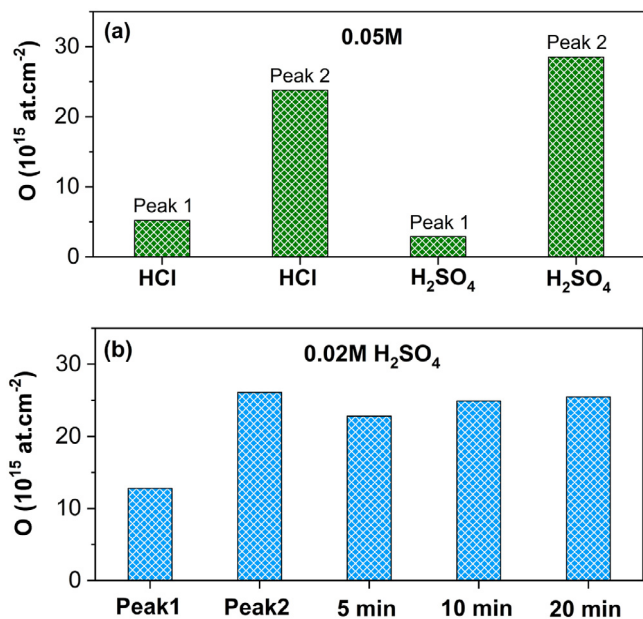


Fig. 6. Surface oxygen concentration (atoms cm^{-2}) obtained from ToF-ERDA measurements after a potential scan through the two anodic oxide peaks for n-type InP in 0.05 M HCl and 0.05 M H₂SO₄ solution (a) with respective potentials corresponding to $U = 0.37$ V and $U = 1.75$ V. The maximum light intensity was used. In (b) potential scan results for unilluminated p-type InP in 0.02 M H₂SO₄ solution are shown for the two peak regions. The influence of time was determined after stepping the potential from OCP to the second peak region.

in all cases composed mainly of the stoichiometric phases InPO₄ and In(PO₃)₃. The contribution of amorphous In(PO_y)_x was about 25%. The In 3d results agree with these trends. Small Cl concentrations of about 0.2 at.% were detected on the HCl-treated samples. Although the overall composition was similar for the two anodic peaks, the In(PO₃)₃/P_{ox} ratio was larger for the second peak. A comparison of the surface sensitive versus the bulk sensitive spectra showed no significant depth dependence indicating that oxide composition was uniform throughout the film. In contrast to anodic oxides grown in non-acidic electrolytes, the typical In_{ox}-rich cap on top of the P_{ox}-rich layer was not observed in this work [33,48,50].

ToF-ERDA results for the potential scan experiments are shown in Fig. 6(a). The measurements for the first photoanodic peak in 0.05 M HCl (the potential was scanned from -0.5 V to $+0.37$ V) indicated an oxygen coverage of $5 \text{ E}+15 \text{ cm}^{-2}$. A lower areal O density of $3 \text{ E}+15 \text{ cm}^{-2}$ was observed for 0.05 M H₂SO₄. This result was supported by the corresponding XPS spectra that showed a lower oxide contribution in the higher binding energy range as compared to the HCl case. When the potential was scanned further through the second peak and interrupted at $+1.75$ V, a significant increase in the oxygen areal density was noted: $24 \text{ E}+15 \text{ cm}^{-2}$ and $28 \text{ E}+15 \text{ cm}^{-2}$ for 0.05 M HCl and H₂SO₄, respectively. In a potential-scan experiment with p-type InP in 0.02 M H₂SO₄ solution (Fig. 6(b)), the O coverage was $13 \text{ E}+15 \text{ cm}^{-2}$ for the first anodic peak and increased to $26 \text{ E}+15 \text{ cm}^{-2}$ for the second peak.

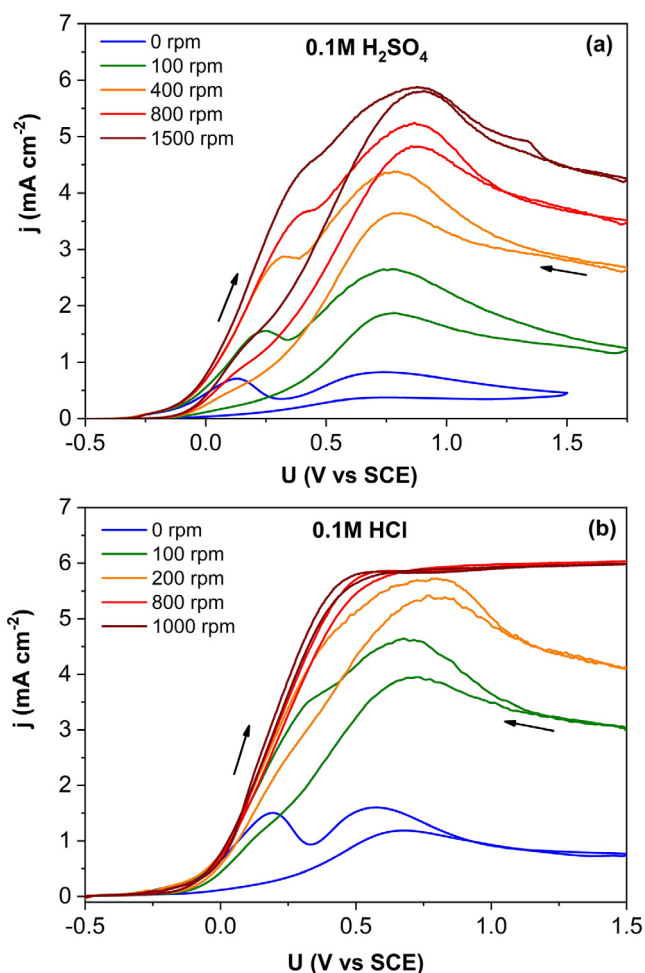


Fig. 7. Current density-potential plots for an n-type InP RDE recorded at maximum light intensity (100%) and different rotation rates in (a) 0.1 M H₂SO₄ and (b) 0.1 M HCl solution.

When the potential was stepped from OCP to the second anodic peak region, the coverage after 5 min was $23 \text{ E}+15 \text{ cm}^{-2}$ and was slightly higher for the longer polarization times of 10 and 20 min: $25 \text{ E}+15 \text{ cm}^{-2}$.

3.3. Hydrodynamics

That mass transport in solution plays an important role in photoanodic oxidation of InP in acidic solution was shown by experiments with an n-type InP RDE. Fig. 7(a) gives results for a 0.1 M H₂SO₄ experiment. The most important feature here is the marked increase in current density in the entire potential range as the rotation rate is increased. There are also other differences. While two distinctive peaks with approximately the same current maximum are clear in the voltammogram of the stationary electrode, at the lowest rotation rate of the RDE (100 rpm) the first peak is less well

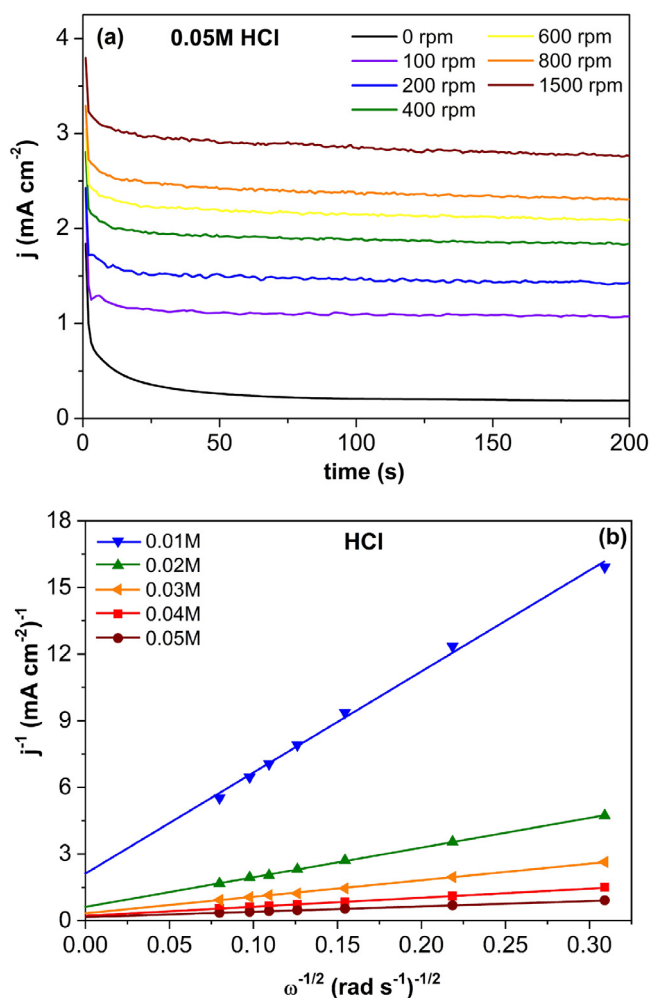


Fig. 8. (a) Time dependence of the current density for an n-type InP RDE following a potential step from open circuit to $U = 0.6$ V (vs SCE) as a function of electrode rotation rate at maximum light intensity (100%). Corresponding Koutecky-Levich plots are shown in (b). For the analysis, the (quasi)steady-state current density was used for $t = 125$ s.

defined and its maximum is considerably lower than that of the second peak. As the rotation rate is further increased to 200 rpm, the first peak becomes a “plateau” while, at the highest rotation rate, it merges with the second peak. It is also striking that (i) the hysteresis in the return scan in the potential range of the second peak is reduced as the rotation rate is increased and (ii) the maximum current density at 1500 rpm is that expected for the light intensity used (100%) (compare with Fig. 1). Although general trends for the corresponding experiments with 0.1 M HCl (Fig. 7(b)) are similar to those found with 0.1 M H_2SO_4 , there are important differences. The first peak, clear at 0 rpm, disappears more rapidly on rotation of the electrode (at 100 rpm a peak is no longer visible). At 200 rpm the current density of the second peak maximum is close to that expected on the basis of light intensity, while at the two highest rotation rates (800, 1000 rpm) an almost “ideal” photocurrent-potential curve is found with the expected limiting photocurrent. It is clear that hysteresis in the return scan through the second peak decreases as the rotation rate is increased, disappearing entirely at the highest rotation rates. Strong hysteresis is observed in the return scan through the potential range of the first peak for H_2SO_4 at all rotation rates and for HCl only at 100 and 200 rpm.

In order to study the influence of rotation rate on the kinetics of anodic oxidation, potential-step measurements were performed for both acids. The electrode potential was stepped (at $t = 0$) from the

open-circuit value to a potential in the range of the second peak (+0.6 V). The photocurrent was measured as a function of time. Fig. 8 shows the result for a 0.05 M HCl solution. On application of the potential there is a rapid drop in photocurrent, followed by a slow decay for both the stationary and the rotating electrode. The effect of rotation is evident: the establishment of a (quasi)steady-state current is slower for the stationary electrode and this current increases strongly with increasing rotation rate (the value of 1500 rpm is a factor of 14 higher than that at 0 rpm). Similar results were found for 0.05 M H_2SO_4 solution (Figure S5).

A plot of the Levich equation [51] showing the steady-state current as a function of the square root of the rotation rate does not give a straight line for these results. This indicates that the steady state is not determined solely by mass transport in solution; the kinetics of an interfacial reaction also plays a role. An analysis based on the Koutecky-Levich equation [51,52] allows us to distinguish between these contributions:

$$\frac{1}{j} = \frac{1}{j_K} + \frac{1}{j_D} = \frac{1}{j_K} + \frac{1}{a\sqrt{\omega}} \quad (2)$$

Here j is the measured current density, j_K is the contribution from the surface reaction and j_D that resulting from mass transport. The latter is, as in the Levich equation, proportional to the square root of the rotation rate ω (rad s^{-1}) (“ a ” in this equation is a constant, directly proportional to the concentration of the species responsible for mass transport control.) Despite the obvious complexity of the chemistry involved in this system (see also discussion) it is clear that the HCl results shown in Fig. 8(b) conform to a Koutecky-Levich analysis. Plots of $1/j$ versus $1/\sqrt{\omega}$ give straight lines whose intercept on the current axis yields a value for $1/j_K$ for the various acid concentrations (0.01–0.05 M). Clearly, j_K depends on the proton concentration (see Fig. 9(a)). By subtracting $1/j_K$ from $1/j$ one can obtain the mass transport component j_D . Fig. 9(b) shows that plots of j_D versus $\sqrt{\omega}$ give straight lines (as expected from the Levich equation). The slope of these lines is clearly dependent on the acid concentration. An analysis of the result of experiments with 0.05 M H_2SO_4 (see Figure S6) shows trends similar to those described above for HCl. We shall consider these results further in the discussion section.

Since mass transport plays an important role in the oxidation reaction, one might expect potential-scan rate to be important in determining the cyclic voltammogram [51]. Fig. 10 shows that this is indeed the case. For experiments with 0.1 M acids, an increase in scan rate from 2 to 100 mV s^{-1} leads to a very significant increase in current in the whole potential range. The shape of the voltammogram remains essentially unchanged. As in previous experiments, the current for 0.1 M HCl was markedly higher than that for 0.1 M H_2SO_4 (at the same scan rate). For a simple irreversible redox reaction, one expects the peak current density j_p to be proportional to the square root of the scan rate of the potential. Figure S7 shows that, in the present complex system, results for the first peak approach this dependence. The dashed straight lines correspond to “ideal” behavior.

4. Discussion

4.1. General features

The present study shows that n-type InP, in contrast to n-type GaAs, can undergo passivation during anodic polarization at relatively low current density. Three factors are important: the light intensity, the nature of the acid and its concentration, and the hydrodynamics of the system. In the case of GaAs, a potential-independent limiting photocurrent is observed that is (i) directly proportional to light intensity up to relatively high values of the photon flux and (ii) independent of acid concentration down to 0.01 M for both HCl and H_2SO_4 (Fig. 2). In 1 M HCl, n-type InP

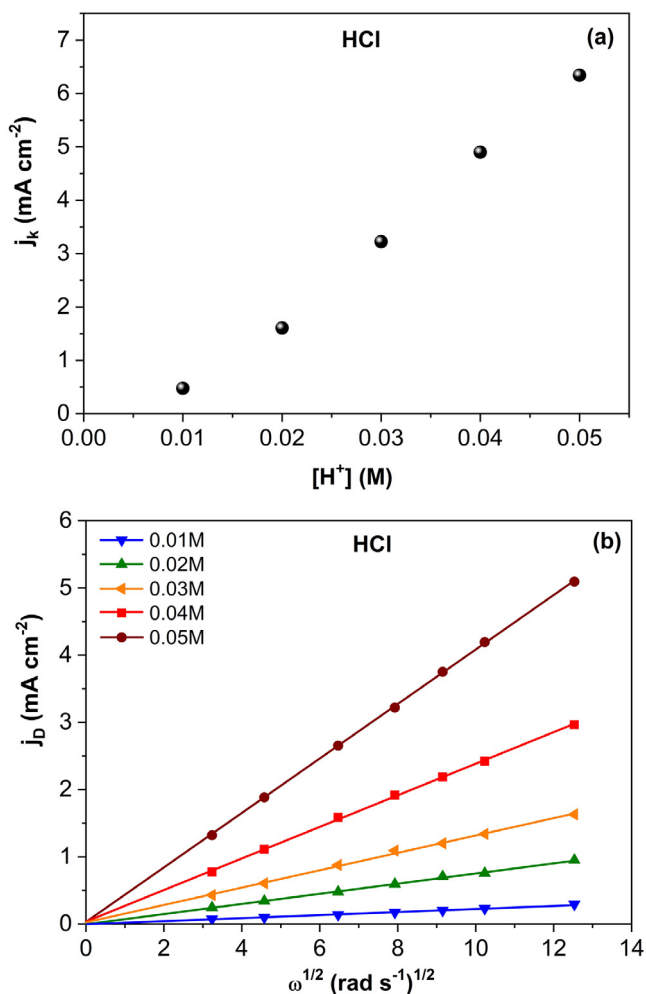


Fig. 9. (a) Plot of the current density attributed to the kinetics of the surface reaction j_k as a function of the proton concentration as obtained from Koutecky-Levich analysis. (b) Corresponding current density due to mass transport j_D versus the square root of the rotation rate for different concentrations of HCl.

remains active up to photocurrent densities comparable to those encountered with GaAs (Fig. 1a). On the other hand with 1 M H₂SO₄, hysteresis in the cyclic voltammograms indicates oxide formation at higher light intensity (Fig. 1b). As the concentration of both acids is lowered (Figs. 3 and 4), passivation is revealed by two peaks in the current-potential plots and by photocurrent densities considerably lower than those expected on the basis of the light intensity.

ToF-ERDA measurements confirmed oxide formation on InP in the potential range of the two peaks of the voltammogram for both acids (Fig. 6). The oxide coverage increased significantly when the potential was scanned through the second anodic peak, in agreement with potential step experiments for a p-type InP electrode. XPS showed the oxide to consist mainly of InPO₄ with additional contributions from In(PO₃)₃, In(PO_y)_x and P₂O₅ (Fig. 5). In addition, some In₂O₃ and elemental phosphorous (P⁰) were also observed.

For active, i.e. oxide-free dissolution of InP as shown for 1 M HCl solution at maximum light intensity (Fig. 1(a)) and 1 M H₂SO₄ at somewhat lower intensity (Fig. 1(b)), our results and those of other workers [20,22,36,37] indicate that 6 charge carriers are required to dissolve one formula unit of the semiconductor. Trivalent products, In³⁺ and H₃PO₃ are formed in solution (Eq. (1)). For both acids at lower proton concentration, as in Figs. 3 and 4, dissolution of the semiconductor occurs via oxide formation (Equations 3a-c)

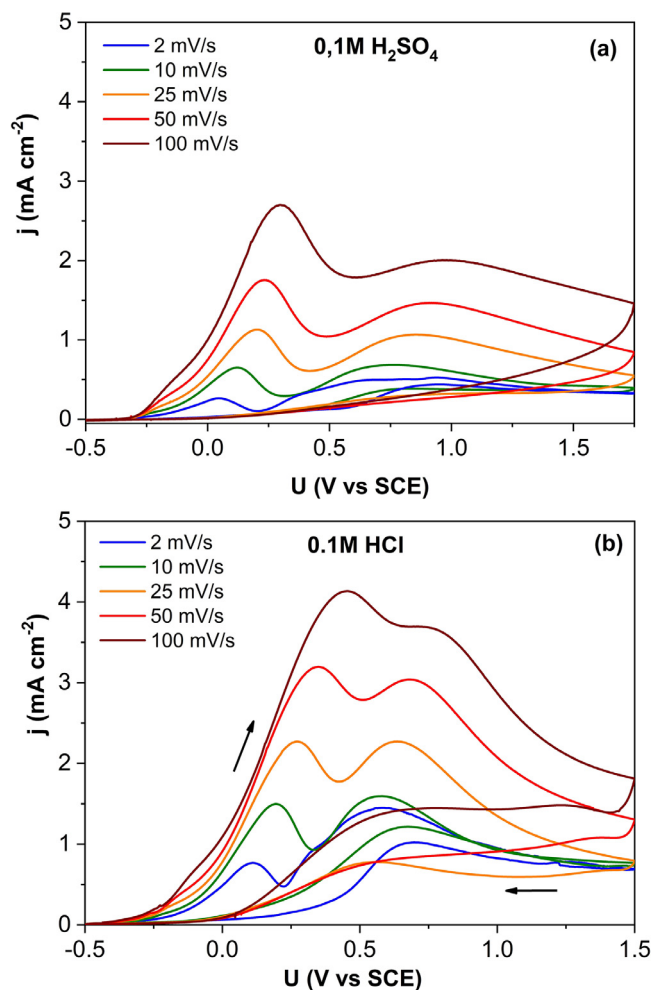
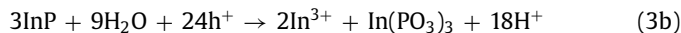
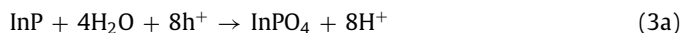
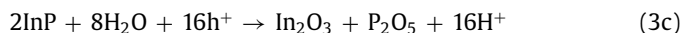


Fig. 10. Influence of scan rate on the current density-potential plots for n-type InP recorded in 0.1 M H₂SO₄ (a) and 0.1 M HCl solution (b).

and dissolution (Equations 6a-d). That the XPS results reveal an oxide consisting predominantly of pentavalent P (InPO₄, In(PO₃)₃ and P₂O₅) indicates that oxidation requires 8, instead of 6 charge carriers per InP unit. Formation of the mixed oxides, InPO₄ and In(PO₃)₃, can be described by Eq. (3a) and 3b



In both cases 8 holes are involved per InP unit. The InPO₄ reaction produces 8 protons and polyphosphate 6 per oxidized InP. With a stoichiometry close to that of In(PO₃)₃, we assume that the amorphous In(PO_y)_x is formed in a similar way [30,31]. The reaction giving rise to In₂O₃ and P₂O₅ is described by

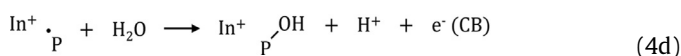
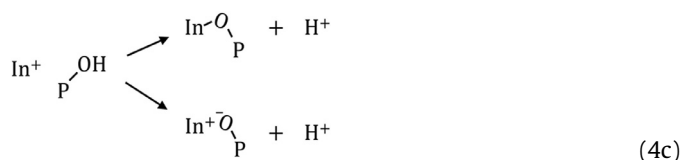
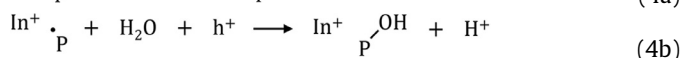


Here, as for InPO₄, 8 holes are required and 8 protons are transferred to solution. In₂O₃ can also result from a chemical reaction of In³⁺ ions (see Eq. (3b)) with water). In contrast to the above examples, the formation of elemental phosphorous requires 3 holes per InP unit and protons are not involved in the reaction



Such a form of preferential oxidation of the group III element was also observed for other III-V semiconductors [5,38,39].

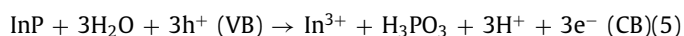
An important step in the growth of these mixed In/P oxides must be the creation of an In-O-P bridge that anchors the In and P atoms in the lattice. This process can be visualized in a simplistic scheme by a series of basic steps [18,20,36]



In the first step (Eq. (4a)) a photogenerated hole is localized in an InP surface bond. The resulting electron-deficient bond, after capture of a second hole, reacts with a water molecule, thus completing bond rupture (Eq. (4b)). Condensation of the resulting In⁺ and P-OH entities with the release of a proton (Eq. (4c)) gives an oxygen bridge (represented here in two forms: covalent and ionic).

Two different pathways for further oxidation are possible. If, following step 4b, the back bonds to the In and P surface atoms undergo a similar sequence (4a + 4b) before bridge formation can occur, then the In and P atoms will pass into solution as In³⁺ and P(OH)₃ that converts to the diprotic acid form, HPO(OH)₂ [53]. This pathway corresponds to “active” dissolution, as encountered with InP in 1 M HCl at full light intensity and 1 M H₂SO₄ at lower light intensity (Fig. 1). If, on the other hand, the back bonds from already bridged surface atoms undergo similar bridge formation (as in 4c) then an oxide matrix can be formed. While active dissolution of InP gives rise to a P³⁺ product in solution (Eq. (1)), P atoms fixed in the oxide can be further oxidized to P⁵⁺ as detected in the XPS measurements.

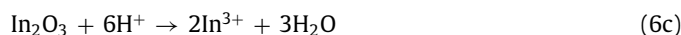
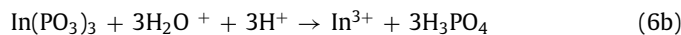
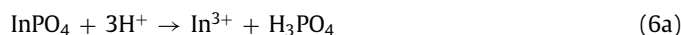
An intermediate with unpaired electron, such as that formed in step 4a, is equivalent to a surface state with an energy in the bandgap of the semiconductor [54]. The electron can be thermally injected into the conduction band and, with a low concentration of holes in the valence band (i.e. at low light intensity [36]), this step can compete with 4b, capture of a second hole. When this combination of steps 4a and 4d is repeated 3 times, then only 3 instead of 6 photons are required to oxidize one unit of InP [36]



This corresponds to a quantum efficiency (QE) of 2, i.e., two charge carriers are generated per absorbed photon. This effect, referred to as photocurrent doubling, is observed only at a light intensity considerably lower than that used in the present work [36]. Some enhancement of the photocurrent ($2 > \text{QE} > 1$) might be expected at the lowest light intensity. However, it is not clear to what extent surface oxide will influence photocurrent multiplication. Oxide formation leads to a drop in photocurrent below the value expected on the basis of the photon flux. This is accompanied by an increase in electron-hole recombination. The study of electron injection from bandgap states will, under these circumstances, be complicated. However, whether two holes or a hole plus an electron are responsible for bond rupture is not important in the present argument regarding active versus passive oxidation.

The strong dependence of anodic current on the pH of the electrolyte solution indicates that protons must influence the solubility

of the oxide product. The dissolution reactions for the various oxides can be described by



Three protons are required for each In³⁺ passing into solution in all cases. Phosphorous pentoxide should hydrolyze on exposure to water



Phosphoric acid (H₃PO₄) and phosphorous acid (H₃PO₃) will dissociate in solution. The extent of hydrolysis, a reaction that releases protons to solution, depends on the pH of the solution.

From the potential-scan and the potential-step measurements with a rotating disk electrode it is clear that hydrodynamics is important in determining the kinetics of anodic oxidation and layer formation. At lower acid concentration, the current density is influenced markedly by both the electrode rotation rate and the potential scan rate in the complete potential range of the peaks for the two acids (Figs. 7 and 10). This raises the question as to the species in solution that is responsible for mass-transport control. The steady-state results of Fig. 9(b) and S6(b), showing that the slope of j_D versus $\sqrt{\omega}$ plots depends on acid concentration, suggests that the concentration of protons at the surface is important. It is clear that while protons are consumed at the interface during oxide dissolution, they are replenished by the oxidation reactions. In the case of InPO₄ formation (Eq. (3a)) 8 protons are produced per InP unit that is oxidized, while only 3 protons are involved in etching InPO₄ (Eq. (6a)). So the net reaction produces 5 protons, a number that will be higher as H₃PO₄ dissociates. A similar positive proton balance is also expected for the other oxide forms: In(PO₃)₃ and In₂O₃ (Equations 3b,c). It is therefore unlikely that proton depletion occurs at the solid/solution interface. Further evidence for this conclusion is provided by the dependence of the diffusion current j_D on the pH. If protons determine mass transport, then, for a given rotation rate, j_D should be directly proportional to the proton concentration: $j_D = k_D[\text{H}^+]^n$ with $n = 1$ [51]. Fig. 9(b) shows that the exponent “n” is considerably higher than 1. This also holds for the H₂SO₄ results (Figure S6). In addition, since the proton has a large diffusion coefficient [55], one would expect markedly higher values for j_D than those shown in Fig. 9(b) (and Figure S6). Consequently, we conclude that, while pH is important in determining oxide solubility, removal of products of InP oxidation and of oxide dissolution from the solid/solution interface to the bulk solution determines the hydrodynamics of the present system.

The present reaction scheme involving oxidation of InP, initial passivation, oxide growth and dissolution, and diffusion of reaction products to the bulk solution is, with the results now available, too complex to analyze in terms of Koutecky-Levich kinetics. However, it should be noted that Eq. (2) can apply to an electrode reaction in which the hydrodynamics is determined by mass transport of product. This can be the case for a process involving a surface reaction, dissolution and mass transport in which the product is sparingly soluble and blocks the electrode reaction [56].

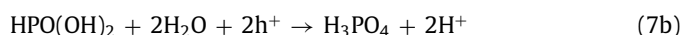
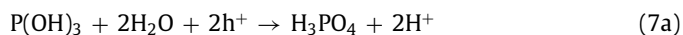
4.2. The InP/H₂SO₄ system

The conclusions drawn in the previous section provide a basis for a qualitative understanding of the chemistry encountered during the potentiodynamic scans. We focus first on the case of

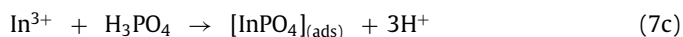
a stationary n-type InP electrode at maximum light intensity in 0.1 M H₂SO₄ (Fig. 3(b), 100%). Three potential ranges can be distinguished in the forward scan of the voltammogram. As the potential is made positive with respect to the open-circuit value, the current initially increases sharply (range I). However, instead of a potential-independent limiting photocurrent, the voltammogram shows a peak typical of oxide formation (range II). The maximum current in the peak is a factor of approximately 8 lower than that expected on the basis of light intensity (compare with Fig. 1(a), 100%). After passing through a minimum, the current again increases, giving a second peak (range III), with a maximum current density slightly higher than that of the first peak. A marked hysteresis is observed in the return scan to negative potential.

The results obtained with a rotating disk electrode (Fig. 7(a)) provide information on the transition from active dissolution at lower current density (range I) to passivation (range II). At the lowest rotation rate of 100 rpm, a peak is also seen, but with a maximum current twice that found for the stationary electrode. At 400 rpm, the current corresponding to the plateau that replaces the first peak is a factor of approximately 2 higher than that at 100 rpm. This current continues to increase with increasing rotation rate. At 1500 rpm, the inflection point has a value (4.5 mA cm⁻²), close to that expected on the basis of the light intensity. The limiting value of 6 mA cm⁻² is, in fact, reached in the second peak. This suggests that, in this case, the surface is essentially oxide-free. The decrease in current beyond the peak maximum indicates a return of some oxide. From Fig. 7(a) it is clear that the critical current density required for the transition from "active" dissolution of InP to oxide formation and possible passivation is dependent on the hydrodynamics of the system.

Anodic oxidation of the semiconductor in the active range I gives rise to In³⁺ and P(OH)₃/HPO(OH)₂ at the solid/solution interface (Eq. (1)). In the previous section we concluded that hydrodynamics in the present system is determined by mass transport of oxidation products from the surface to the bulk solution. With a stationary electrode in an unstirred solution (e.g. Fig. 3(a), 100%) the rate of removal of reaction products from the surface will be limited. As a result, at constant potential the concentration of these products will build up at the surface until a steady state is achieved (the rate of formation = rate of removal via diffusion/convection). This suggests a possible mechanism for explaining the onset of the transition from active dissolution (range I) to passivation (range II). This involves the further anodic oxidation of the primary trivalent group V product, either the as-formed P(OH)₃ or the converted stable diprotic form, to give pentavalent phosphate:



In the presence of a relatively high In³⁺ concentration at the surface, InPO₄ can be formed [42,53]:



Adsorbed at the interface, InPO₄, the main component of the passive layer, may block the surface, thus hindering active dissolution (Eq. (4b) and following steps). This favours oxide formation and passivation (Eq. (4c)). It is clear that, on rotation of the electrode, removal of the initial oxidation products from the surface is more effective and passivation should occur at a higher current density. Since solubility of InPO₄ depends on protons (Eq. (6a)) it is not surprising that the current at which the active/passive transition occurs depends on the pH of the solution.

In range II (through the first peak in the voltammogram) an oxide film is formed on the surface. In the case of a stationary elec-

trode in 0.05 M H₂SO₄ this inner layer is about 0.5 nm thick. As a result of oxide growth, the potential distribution at the semiconductor/solution interface is altered. Part of the applied potential now falls over the oxide, providing the electric field required for layer growth. There is a corresponding decrease in the electric field of the space-charge layer in the semiconductor, leading to enhanced electron-hole recombination and a reduced photocurrent. Competition between anodic oxide formation and dissolution determines the shape of the voltammogram. The latter depends on both the proton concentration and solution hydrodynamics. Since InPO₄ and In(PO₃)₃ are the main oxidation products, the charge transfer reactions giving rise to oxide formation (Equations 3a,b) very likely occur at the semiconductor/oxide interface. Under influence of the electric field across the oxide layer, protons migrate to the oxide/solution interface. "Non-bonded" In³⁺ ions (see Eq. (3b)) may also migrate and pass into solution, a process that is not expected for phosphorous bonded to oxygen.

An increase in applied potential beyond that corresponding to the first peak leads to an increase in current and the appearance of a second peak (Fig. 3(b)). The surface oxide continues to grow. For a 0.05 M H₂SO₄ solution, ToF-ERDA results (Fig. 6(a)) show that the oxide coverage at the surface has increased markedly (from 3 E+15 O cm⁻² (range II) to 28 E+15 O cm⁻² (range III)). Hysteresis in the cyclic voltammograms provides information about the oxide in the two ranges. For a stationary electrode in 0.1 M H₂SO₄ (Fig. 3(b)), an essentially constant current is clear in the return scan through range III, that of the second peak. The current drops to a low value in the range of the first peak. The influence of rotation rate on this result is also striking (Fig. 7(a)). While the current in the forward scan increases markedly, hysteresis in the return scan decreases as the rotation rate is raised from 0 to 1500 rpm. These two results can be attributed to an increase in oxide dissolution rate as a result of the enhanced rate of removal of the dissolved product from the surface. As for the stationary electrode, considerable hysteresis is still observed in the range of the first peak. We conclude that the rate of removal of the oxide in the first peak does not keep pace with the rate of change of potential. There is a rapid drop in the electric field across the barrier oxide so that the current quickly drops to a low value. From these results we conclude that an essentially different oxide is associated with each of the current peaks, an inner layer and an outer layer with relatively low and high solubility, respectively.

The present results resemble in a number of respects our previous work on anodic oxidation of SiC, p-type in the dark and n-type under illumination, in acidic fluoride solution [57,58]. A two-peak voltammogram with marked hysteresis in the return scan was also observed for SiC. The strong dependence of current on electrode rotation rate in the potential range of both peaks was attributed to mass-transport limitation due to fluoride ion depletion at the electrode surface. On the basis of surface analysis and electrical impedance measurements it was clear that the results are due to differences in the nature of the oxide. The SiC results were interpreted with a two-layer model, similar to that previously reported for Si in HF solution [52,59–63], a compact SiO₂ inner layer and a thicker less dense outer layer. In the case of Si it was suggested that the outer layer consisted of a hydrated oxide. In the case of SiC the outer layer must be porous in order to account for its thickness (in the micron range). The results for the three semiconductors suggest that, as the potential is increased on going from the first through the second peak, the outer edge of the inner compact oxide undergoes a transition to give a less dense or hydrated oxide, while the inner layer continues to grow at the semiconductor/oxide interface. The mechanism of such a conversion is not clear.

The present results show an interesting contrast in the mechanism of anodic oxidation of the three semiconductors in acidic so-

lution. In the case of Si and SiC the fluoride ion plays a dual role. It acts as complexing agent for Si^{4+} and is essential for oxide dissolution while depletion of fluoride at the solid/solution interface is responsible for mass-transport control. In the case of InP, protons are essential for oxide dissolution (oxide solubility depends on pH) but they are not depleted at the electrode surface. In this case the hydrodynamics is determined by transport of the oxidation products from the electrode surface to the bulk solution.

4.3. The role of Cl^-

Although the general features of the voltammograms for n-type InP in HCl and H_2SO_4 under the same experimental conditions are quite similar, there are some striking differences. While “ideal” photocurrent-potential curves were found for 1 M HCl up to the maximum light intensity (100%) (Fig. 1(a)), this is not the case for 1 M H_2SO_4 . At the higher light intensities (79%, 100%) a peak is observed in the forward scan and significant hysteresis in the return scan (Fig. 1(b)). Only at an intensity of 50% (and lower) was a voltammogram recorded comparable in shape to that for 1 M HCl. At lower acid concentration (0.1 M), for example, two peaks are observed in the forward scan for both acids, with hysteresis in the reverse scan (Fig. 3(a) and (b)). The general level of the photocurrent was considerably higher in the HCl case while there was less hysteresis in the return scan to the second peak maximum. The difference between the results for the two acids at lower molarity (0.01–0.05 M) (Fig. 4) was less pronounced but still evident. An exception is the 0.01 M case. The slightly higher peak current for 0.01 M H_2SO_4 very likely results from the higher proton concentration (0.0144 M).

With rotation of the electrode, the influence of HCl is even more striking. In this case, the first peak in the voltammogram observed for 0.1 M H_2SO_4 at 100 rpm (Fig. 7(a)) has been replaced by a “weak” plateau (Fig. 7(b)). For HCl at 200 rpm the plateau is almost completely absorbed by the second peak, which has a photocurrent maximum close to the value expected for the light intensity (100%). At the two highest rotation rates (800, 1000 rpm) the HCl photocurrent-potential curves resemble the curve for 1 M HCl with a stationary electrode. Again, for HCl at low rotation rate the hysteresis in the return scan through the second peak is less than for H_2SO_4 at the same rotation rate.

The potential scan rate has a similar effect on the voltammograms as rotation rate (Fig. 10). For HCl there is a marked increase in photocurrent in the potential range of the first and second peaks with increasing scan rate (2–100 mVs^{-1}) while the initial hysteresis in the return scan is reduced.

That the Cl^- ion is responsible for the enhanced current in the above examples is supported by an experiment with a stationary InP electrode in a 0.1 M HCl solution in which the chloride concentration was increased to 1 M by addition of KCl (Fig. 11). The photocurrent-potential curve of Fig. 3(b) is changed radically from a 2-peak voltammogram to one showing a potential-independent limiting photocurrent as for 1.0 M HCl. Addition of Cl^- gives the expected limiting photocurrent in a broad potential range with limited hysteresis. As already mentioned in the Results section, we expect the chloride ion to act as complexing agent for In^{3+} [41,42]. If Cl^- “scavenges” the dissolved In^{3+} ions, formation of InPO_4 on the surface (Eq. (7c)) and subsequent passivation are prevented.

The chloride ion can also interfere at two stages in the anodic oxidation of InP (Equations 8a,b). First, it can react with the product of step (4b) by complexing the surface In^+ , thus forming an In-Cl bond (Eq. (8a)). In this way oxygen-bridge formation (step (4c)), an essential step in oxide formation, is thwarted. Second, HCl can be expected to enhance the oxide dissolution rate (with respect to that of H_2SO_4) by a more effective rupture of the oxygen-bridged surface bond (Eq. (8b)).

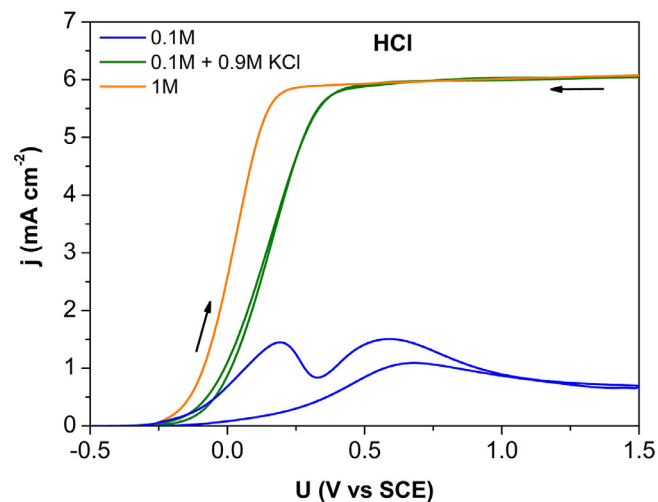
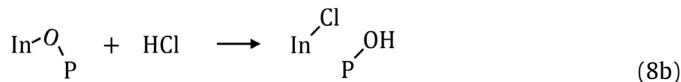
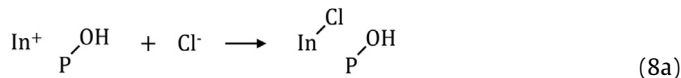


Fig. 11. Current density-potential plots for a stationary n-type InP at maximum light intensity (100%) showing the influence of the Cl^- anion on the cyclic voltammogram.



These two processes also contribute to the significant enhancement of the anodic photocurrent in the case of HCl, as observed for 0.1 M and 0.25 M acid solution (see Figs. 3 and S1). At lower acid concentrations (≤ 0.05 M) the influence of the chloride ion, although less pronounced, is still evident (see Fig. 4). This trend is confirmed on comparing the values of the rate constant for the surface reaction of the two acids in the proton concentration range 0.03 - 0.05 M. The rate constant is higher for HCl than for H_2SO_4 (compare Figs. 9(a) and S6(a)). It then seems surprising that ToF-ERDA shows a higher surface oxygen concentration for the passivating oxide formed in the first peak of the voltammogram in the case of 0.05 M HCl (see Fig. 6). The reason for this result is not clear. The XPS results in Figs. 5 and S3 show that the chemical composition is essentially the same for the two oxides. Possibly, a difference in dielectric properties requires a thicker layer to ensure passivation in HCl solution.

4.4. InP and GaAs: a comparison

In a previous study [17] of the chemical etching of GaAs and InP in acidic solutions containing the strong oxidizing agent H_2O_2 we observed trends similar to those described in the present work. Passivation of InP in both HCl and H_2SO_4 resulted in very low etch rates. The etch rate for HCl was (i) higher than that for the corresponding H_2SO_4 solution and (ii) dependent on both the H_2O_2 and acid concentrations. GaAs, on the other hand, showed a much higher etch rate in H_2SO_4 that was dependent on the H_2O_2 concentration but not on the proton concentration (0.01–1 M). GaAs clearly does not passivate in the H_2SO_4 etchant.

For chemical etching the striking difference in the etching properties of the two semiconductors was attributed to formation of an oxygen bridge between the group III and the group V atoms (see Eq. (4c)). It was suggested that formation of such an In-O-P bridge is more favourable than that of a Ga-O-As bond due to

the ease with which a proton can be removed from the P atom (Eq. (4c)), as compared to the As atom. This trend also seems to hold for anodic etching for III-V semiconductors. We have found that photoanodic etching of InGaAs is similar to that of GaAs in that passivation is not observed even at low acid concentrations. Figure S8 shows voltammograms for a 0.01 M HCl solution with a well-defined limiting photocurrent and no indication of oxide formation. In the work of Menezes and Miller it was indicated that p-type and illuminated n-type GaAs was only passivated in 1 M H₂SO₄ at high current densities above 100 mA cm⁻²[64]. On the other hand Goossens and Gomes have shown that anodic polarization of n-type GaP under illumination in H₂SO₄ (pH = 1) in a flow-cell experiment gives a passivation peak with a maximum comparable to that of InP in this work[65]. Also passivation is not observed at low light intensity. As in the case of InP, considerable hysteresis, reported for the return scan is substantially reduced when the electrode is rotated at 1200 rpm, indicating the importance of hydrodynamics. Such results indicate that in the case of chemical and anodic etching of these III-V semiconductors in acidic solution the chemistry of the group V atom is especially important.

5. Summary and conclusions

At the maximum light intensity used in this work, corresponding to a limiting photocurrent density of 6 mA cm⁻², typical anodic photocurrent-potential characteristics were observed for both n-type InP and GaAs in 1 M HCl solution. On the other hand, for InP in 1 M H₂SO₄ hysteresis in the cyclic voltammogram indicated the formation of a surface layer. In contrast to GaAs, at lower proton concentration InP undergoes passivation during photoanodic oxidation in both acids. Cyclic voltammograms revealed two anodic peaks when the potential was scanned from the open-circuit value to positive potentials. The current corresponding to the two peaks decreased markedly as the acid concentration was lowered from 0.1 M to 0.01 M. The maximum current density in both peaks was systematically higher for HCl than for H₂SO₄. Rotation of the electrode leads to a considerable increase in current in the whole potential range and to a reduction in the current hysteresis in the range of the second peak (that at higher potential). XPS and ToF-ERDA measurements were used to obtain information about the chemical composition of the oxide and its thickness.

A Koutecky-Levich analysis of steady-state current as a function of electrode rotation rate showed that the kinetics of oxide formation/dissolution is determined by both the surface reactions and mass transport in solution. Although protons are important for oxide dissolution, they are not depleted at the electrode surface. We conclude that removal of the oxidation products from the solid/solution interface accounts for mass transport in the system.

The results are considered on the basis of a bilayer model, an inner compact layer and a less dense outer layer. A simple reaction scheme showing the initial steps in combination with total oxidation and dissolution reactions was used to explain the competition between the two reaction paths (active dissolution and passivation) as well as the special role of the Cl⁻ ion in the kinetics. Finally, we speculate on how mass transport of the oxidation products might influence so strongly the onset of passivation.

Declaration of Competing Interest

The authors declare that they have no known competing financial interests or personal relationships that could have appeared to influence the work reported in this paper.

CRedit authorship contribution statement

Dennis H. van Dorp: Conceptualization, Visualization, Writing - review & editing. **Genis Vanheusden:** Visualization, Data curation. **Kris Paulussen:** Visualization, Data curation. **Ibrahim Hassan:** Visualization, Data curation. **Simon Van Wonterghem:** Visualization, Data curation. **Graniel H. Abrenica:** Visualization, Data curation. **Praveen Dara:** Visualization, Data curation. **Johan Meerschaert:** Visualization, Data curation. **Thierry Conard:** Visualization, Data curation. **Frank Holsteyns:** Supervision. **John J. Kelly:** Writing - review & editing.

Acknowledgments

This work is part of the imec Industrial Affiliation Program on III-V/Ge devices. The authors acknowledge Screen Semiconductor Solutions Co. Ltd., Entegris ATMI, Kurita and Fuji Film Electronic Materials for their contributions to the Joint Development Program. We wish to thank Anja Vanleenhove for supporting the XPS measurements and Dr. Jean-Noël Chazalviel for his suggestions regarding Koutecky-Levich kinetics.

Supplementary materials

Supplementary material associated with this article can be found, in the online version, at doi:[10.1016/j.electacta.2020.136872](https://doi.org/10.1016/j.electacta.2020.136872).

References

- [1] L. Gao, Y. Cui, J. Wang, A. Cavalli, A. Standing, T.T.T. Vu, M.A. Verheijen, J.E.M. Haverkort, E.P.A.M. Bakkers, P.H.L. Notten, Photoelectrochemical hydrogen production on InP nanowire arrays with molybdenum sulfide electrocatalysts, *Nano Lett.* 14 (2014) 3715–3719, doi:[10.1021/nl404540f](https://doi.org/10.1021/nl404540f).
- [2] N. Kornienko, N.A. Gibson, H. Zhang, S.W. Eaton, Y. Yu, S. Aloni, S.R. Leone, P. Yang, Growth and photoelectrochemical energy conversion of Wurtzite indium phosphide nanowire arrays, *ACS Nano* 10 (2016) 5525–5535, doi:[10.1021/acsnano.6b02083](https://doi.org/10.1021/acsnano.6b02083).
- [3] W.S. Ko, I. Bhattacharya, T.-T.D. Tran, K.W. Ng, S. Adair Gerke, C. Chang-Hasnain, Ultrahigh responsivity-bandwidth product in a compact InP nanopillar phototransistor directly grown on silicon, *Sci. Rep.* 6 (2016) 33368, doi:[10.1038/srep33368](https://doi.org/10.1038/srep33368).
- [4] C.-W. Cheng, K.-T. Shiu, N. Li, S.-J. Han, L. Shi, D.K. Sadana, Epitaxial lift-off process for gallium arsenide substrate reuse and flexible electronics, *Nat. Commun.* 4 (2013) 1577, doi:[10.1038/ncomms2583](https://doi.org/10.1038/ncomms2583).
- [5] N.J. Smeenk, J. Engel, P. Mulder, G.J. Bauhuis, G. Bissels, J.J. Schermer, E. Vlieg, J.J. Kelly, Arsenic formation on GaAs during etching in HF solutions: relevance for the epitaxial lift-off process, *ECS J. Solid State Sci. Technol.* 2 (2013) P58–P65.
- [6] J.A. del Alamo, Nanometre-scale electronics with III-V compound semiconductors, *Nature* 479 (2011) 317–323, doi:[10.1038/nature10677](https://doi.org/10.1038/nature10677).
- [7] M. Paladugu, C. Merckling, R. Loo, O. Richard, H. Bender, J. Dekoster, W. Vandervorst, M. Caymax, M. Heyns, Site selective integration of III-V materials on Si for nanoscale logic and photonic devices, *Cryst. Growth Des.* 12 (2012) 4696–4702, doi:[10.1021/cg300779v](https://doi.org/10.1021/cg300779v).
- [8] N. Waldron, C. Merckling, L. Teugels, P. Ong, S.A.U. Ibrahim, F. Sebaai, A. Pourghaderi, K. Barla, N. Collaert, A.V.-Y. Thean, InGaAs Gate-All-around nanowire devices on 300mm Si substrates, *IEEE Electron. Device Lett.* 35 (2014) 1097–1099, doi:[10.1109/LED.2014.2359579](https://doi.org/10.1109/LED.2014.2359579).
- [9] K. Tomioka, M. Yoshimura, T. Fukui, A III-V nanowire channel on silicon for high-performance vertical transistors, *Nature* 488 (2012) 189–192, doi:[10.1038/nature11293](https://doi.org/10.1038/nature11293).
- [10] Z. Wang, B. Tian, M. Pantouvaki, W. Guo, P. Absil, J. Van Campenhout, C. Merckling, D. Van Thourhout, Room-temperature InP distributed feedback laser array directly grown on silicon, *Nat. Photonics* 9 (2015) 837–842, doi:[10.1038/nphoton.2015.199](https://doi.org/10.1038/nphoton.2015.199).
- [11] B. Tian, Z. Wang, M. Pantouvaki, P. Absil, J. Van Campenhout, C. Merckling, D. Van Thourhout, Room temperature O-band DFB laser array directly grown on (001) silicon, *Nano Lett.* 17 (2017) 559–564, doi:[10.1021/acs.nanolett.6b04690](https://doi.org/10.1021/acs.nanolett.6b04690).
- [12] Y. Shi, Z. Wang, J. Van Campenhout, M. Pantouvaki, W. Guo, B. Kunert, D. Van Thourhout, Optical pumped InGaAs/GaAs nano-ridge laser epitaxially grown on a standard 300-mm Si wafer, *Optica* 4 (2017) 1468, doi:[10.1364/OPTICA.4.001468](https://doi.org/10.1364/OPTICA.4.001468).
- [13] B. Kunert, W. Guo, Y. Mols, B. Tian, Z. Wang, Y. Shi, D. Van Thourhout, M. Pantouvaki, J. Van Campenhout, R. Langer, K. Barla, III/V nano ridge structures for optical applications on patterned 300mm silicon substrate, *Appl. Phys. Lett.* 109 (2016) 091101, doi:[10.1063/1.4961936](https://doi.org/10.1063/1.4961936).

- [14] S. Uvin, S. Kumari, A.D. Groote, S. Verstuylt, G. Lepage, P. Verheyen, J.V. Campenhout, G. Morthier, D.V. Thourhout, G. Roelkens, 1.3 μm InAs/GaAs quantum dot DFB laser integrated on a Si waveguide circuit by means of adhesive die-to-wafer bonding, *Opt. Express*, OE. 26 (2018) 18302–18309, doi:10.1364/OE.26.018302.
- [15] K.J. Kanarik, T. Lill, E.A. Hudson, S. Sriraman, S. Tan, J. Marks, V. Vahedi, R.A. Gottscho, Overview of atomic layer etching in the semiconductor industry, *J. Vacu. Sci. Technol. A Vac. Surf. Films* 33 (2015) 020802, doi:10.1116/1.4913379.
- [16] G.S. Oehrlein, D. Metzler, C. Li, Atomic layer etching at the tipping point: an overview, *ECS J. Solid State Sci. Technol.* 4 (2015) N5041–N5053, doi:10.1149/2.0061506jss.
- [17] D.H. van Dorp, S. Arnauts, M. Laitinen, T. Sajavaara, J. Meersschaut, T. Conard, J.J. Kelly, Nanoscale etching of III-V semiconductors in acidic hydrogen peroxide solution: GaAs and InP, a striking contrast in surface chemistry, *Appl. Surf. Sci.* 465 (2019) 596–606, doi:10.1016/j.apsusc.2018.09.181.
- [18] J.J. Kelly, P.H.L. Notten, Surface charging effects during photoanodic dissolution of n - GaAs electrodes, *J. Electrochem. Soc.* 130 (1983) 2452, doi:10.1149/1.2119612.
- [19] D. Vanmaekelbergh, W.P. Gomes, F. Cardon, Studies on the n-GaAs photoanode in aqueous electrolytes. 1. Behaviour of the photocurrent in the presence of a stabilizing agent, *Berichte Der Bunsenges. Für Phys. Chem.* 89 (1985) 987–994, doi:10.1002/bbpc.19850890912.
- [20] P.H.L. Notten, J.E.A.M. Meerakker, J.J. Kelly, *Etching of III-V semiconductors: an Electrochemical Approach*, Elsevier Advanced Technology, 1991.
- [21] M.V. Lebedev, W. Calvet, T. Mayer, W. Jaegermann, Photoelectrochemical processes at n-GaAs(100)/aqueous HCl electrolyte interface: a synchrotron photoemission spectroscopy study of etched electrodes, *J. Phys. Chem. C* 118 (2014) 12774–12781, doi:10.1021/jp500564c.
- [22] S. Preusser, M. Herlem, A. Etcheberry, J. Jaume, The photodissolution of InP, *Electrochim. Acta* 37 (1992) 289–295, doi:10.1016/0013-4686(92)85015-D.
- [23] M.P. Besland, In Situ Studies of the Anodic Oxidation of Indium Phosphide, *J. Electrochem. Soc.* 140 (1993) 104, doi:10.1149/1.2056067.
- [24] Z. Hens, W.P. Gomes, Photoanodic Dissolution of n-InP: An Electrochemical Impedance Study, *J. Phys. Chem. B* 104 (2000) 7725–7734, doi:10.1021/jp0010740.
- [25] P. Schmuki, L. Santinacci, T. Djenizian, D.J. Lockwood, Pore Formation on n-InP, *Phys. Status Solidi (A)* 182 (2000) 51–61, doi:10.1002/1521-396X(200011)182:1(51::AID-PSSA51)3.0.CO;2-S.
- [26] H. Tsuchiya, M. Huppe, T. Djenizian, P. Schmuki, Electrochemical formation of porous superlattices on n-type (100) InP, *Surf. Sci.* 547 (2003) 268–274, doi:10.1016/j.susc.2003.10.032.
- [27] P. Schmuki, U. Schlierf, T. Herrmann, G. Champion, Pore initiation and growth on n-InP(100), *Electrochim. Acta* 48 (2003) 1301–1308, doi:10.1016/S0013-4686(02)00839-3.
- [28] A. Eb, A.-M. Gonçalves, L. Santinacci, C. Mathieu, A. Etcheberry, Anodic behavior and pore growth of n-InP in acidic liquid ammonia, *C. R. Chim.* 11 (2008) 1023–1029, doi:10.1016/j.crci.2008.02.002.
- [29] L. Santinacci, M. Bouttey, M. Petit, A.-M. Gonçalves, N. Simon, J. Vigneron, A. Etcheberry, Investigations of the anodic porous etching of n-InP in HCl by atomic absorption and X-ray photoelectron spectroscopies, *J. Electrochem. Soc.* 165 (2018) H3131–H3137, doi:10.1149/2.0181804jes.
- [30] G. Hollinger, J. Joseph, Y. Robach, E. Bergignat, B. Commere, P. Viktorovitch, M. Froment, On the chemistry of passivated oxide-InP interfaces, *J. Vac. Sci. Technol. B Microelectron. Process. Phenom.* 5 (1987) 1108–1112.
- [31] M. Faur, M. Faur, D.T. Jayne, M. Goradia, C. Goradia, XPS investigation of anodic oxides grown on p-type InP, *Surf. Interface Anal.* 15 (1990) 641–650, doi:10.1002/sia.740151102.
- [32] G. Hollinger, R. Skheyta-Kabbani, M. Gendry, Oxides on GaAs and InAs surfaces: An x-ray-photoelectron-spectroscopy study of reference compounds and thin oxide layers, *Phys. Rev. B* 49 (1994) 11159–11167, doi:10.1103/PhysRevB.49.11159.
- [33] T. Djenizian, G... Sproule, S. Moisa, D. Landheer, X. Wu, L. Santinacci, P. Schmuki, M... Graham, Composition and growth of thin anodic oxides formed on InP (100), *Electrochim. Acta* 47 (2002) 2733–2740, doi:10.1016/S0013-4686(02)00138-X.
- [34] A. Pakes, P. Skeldon, G.E. Thompson, S. Moisa, G.I. Sproule, M.J. Graham, Anodic film growth on InP in sodium tungstate, *Corros. Sci.* 44 (2002) 2161–2170, doi:10.1016/S0010-938X(01)00186-X.
- [35] J. Meersschaut, W. Vandervorst, High-throughput ion beam analysis at imec, *Nucl. Instrum. Methods Phys. Res. Sect. B* (n.d.). 10.1016/j.nimb.2017.01.005.
- [36] B.H. Erne, D. Vanmaekelbergh, I.E. Vermeer, The anodic dissolution of InP studied by the optoelectrical impedance method—1. Competition between electron injection and hole capture at InP photoanodes, *Electrochim. Acta* 38 (1993) 2559–2567.
- [37] A.-M. Gonçalves, L. Santinacci, A. Eb, I. Gerard, C. Mathieu, A. Etcheberry, Pore formation on n-InP(100) in acidic liquid ammonia at 223 K: a true water-free etching process, *Electrochem. Solid-State Lett.* 10 (2007) D35, doi:10.1149/1.2434201.
- [38] E.K. Propst, K.W. Vogt, P.A. Kohl, Photoelectrochemical etching of GaSb, *J. Electrochem. Soc.* 140 (1993) 3631–3635.
- [39] R. Memming, G. Schwandt, Electrochemical properties of gallium phosphide in aqueous solutions, *Electrochim. Acta* 13 (1968) 1299–1310, doi:10.1016/0013-4686(68)80058-1.
- [40] F.A. Cotton, G. Wilkinson, C.A. Murillo, M. Bochmann, *Advanced Inorganic Chemistry*, 6th Edition, Wiley, 1999.
- [41] C. Deferm, B. Onghena, T.V. Hoogerstraete, D. Banerjee, J. Luyten, H. Oosterhof, J. Fransaeer, K. Binnemans, Speciation of indium(III) chloro complexes in the solvent extraction process from chloride aqueous solutions to ionic liquids, *Dalton Trans.* 46 (2017) 4412–4421, doi:10.1039/C7DT00618G.
- [42] C.E.A. Brownlow, J.E. Salmon, J.G.L. Wall, 495. Indium phosphates: phase-diagram, ion-exchange, and pH titration studies, *J. Chem. Soc.* (1960) 2452–2457, doi:10.1039/JR9600002452.
- [43] D. Cuyppers, D.H. van Dorp, M. Tallarida, S. Brizzi, T. Conard, L.N.J. Rodriguez, M. Mees, S. Arnauts, D. Schmeisser, C. Adelman, S.D. Gendt, Study of InP Surfaces after Wet Chemical Treatments, *ECS J. Solid State Sci. Technol.* 3 (2014) N3016–N3022, doi:10.1149/2.005401jss.
- [44] D.H. van Dorp, L. Nyns, D. Cuyppers, T. Ivanov, S. Brizzi, M. Tallarida, C. Fleischmann, P. Hönicke, M. Müller, O. Richard, D. Schmeißer, S. De Gendt, D.H.C. Lin, C. Adelman, Amorphous gadolinium aluminate as a dielectric and sulfur for indium phosphide passivation, *ACS Appl. Electron. Mater.* 1 (2019) 2190–2201, doi:10.1021/acsaem.9b00388.
- [45] D. Kikuchi, Y. Matsui, S. Adachi, Chemically treated InP (100) surfaces in aqueous HCl solutions, *J. Electrochem. Soc.* 147 (2000) 1973–1978.
- [46] A. Pakes, P. Skeldon, G.E. Thompson, R.J. Hussey, S. Moisa, G.I. Sproule, D. Landheer, M.J. Graham, Composition and growth of anodic and thermal oxides on InP and GaAs, *Surf. Interface Anal.* 34 (2002) 481–484, doi:10.1002/sia.1343.
- [47] N. Simon, I. Gerard, C. Mathieu, A. Etcheberry, Study of a thin anodic oxide on n-InP by photocurrent transient, capacitance measurements and surface analysis, *Electrochim. Acta* 47 (2002) 2625–2631, doi:10.1016/S0013-4686(02)00123-8.
- [48] N. Simon, N.C. Quach, A.M. Gonçalves, A. Etcheberry, Growth of anodic oxides on n-InP Studied by electrochemical methods and surface analyses, *J. Electrochem. Soc.* 154 (2007) H340, doi:10.1149/1.2709504.
- [49] NIST X-ray Photoelectron Spectroscopy Database, (n.d.). <http://dx.doi.org/10.18434/T4T88K>.
- [50] J. van de Ven, J.J.M. Binsma, N.M.A. de Wild, Formation of stable and highly resistive anodic oxides on InP, *J. Appl. Phys.* 67 (1990) 7568–7571, doi:10.1063/1.345821.
- [51] A.J. Bard, L.R. Faulkner, *Electrochemical Methods: Fundamentals and Applications*, 2001, 2nd ed., Wiley, New York, 2002.
- [52] H.H. Hassan, J.L. Sculfort, M. Etman, F. Ozanam, J.-N. Chazalviel, Kinetic and diffusional limitations to the anodic dissolution of p-Si in fluoride media, *J. Electroanal. Chem.* 380 (1995) 55–61, doi:10.1016/0022-0728(94)03610-F.
- [53] R.C.L. Mooney, Crystal structure of anhydrous indium phosphate and thallic phosphate by X-ray diffraction, *Acta Cryst.* 9 (1956) 113–117, doi:10.1107/S0365110X56000279.
- [54] Rüdiger Memming, *Electrochemical Decomposition of Semiconductors*, in: *Semiconductor Electrochemistry*, John Wiley & Sons, Ltd, 2007, pp. 241–263, doi:10.1002/9783527613069.ch08.
- [55] S.H. Lee, J.C. Rasaiah, Proton transfer and the mobilities of the H⁺ and OH⁻ ions from studies of a dissociating model for water, *J. Chem. Phys.* 135 (2011) 124505, doi:10.1063/1.3632990.
- [56] J.-N. Chazalviel, Private communication, (n.d.).
- [57] D.H. van Dorp, E.S. Kooij, W. Arnoldbik, J.J. Kelly, Electrochemical growth of micrometer-thick oxide on SiC in acidic fluoride solution, *Chem. Mater.* 21 (2009) 3297–3305, doi:10.1021/cm900374s.
- [58] D.H. van Dorp, J.J.H.B. Sattler, J.H. den Otter, J.J. Kelly, Electrochemistry of anodic etching of 4H and 6H-SiC in fluoride solution of pH 3, *Electrochim. Acta* 54 (2009) 6269–6275, doi:10.1016/j.electacta.2009.05.086.
- [59] C. Serre, Characterization of the electropolishing layer during anodic etching of p-type silicon in aqueous HF solutions, *J. Electrochem. Soc.* 141 (1994) 2049, doi:10.1149/1.2055058.
- [60] C. da Fonseca, F. Ozanam, J.-N. Chazalviel, In situ infrared characterisation of the interfacial oxide during the anodic dissolution of a silicon electrode in fluoride electrolytes, *Surf. Sci.* 365 (1996) 1–14, doi:10.1016/0039-6028(96)80111-7.
- [61] J.-N. Chazalviel, Ionic processes through the interfacial oxide in the anodic dissolution of silicon, *Electrochim. Acta* 37 (1992) 865–875, doi:10.1016/0013-4686(92)85038-M.
- [62] M. Bailes, S. Böhm, L.M. Peter, D.J. Riley, R. Greef, An electrochemical and ellipsometric study of oxide growth on silicon during anodic etching in fluoride solutions, *Electrochim. Acta* 43 (1998) 1757–1772, doi:10.1016/S0013-4686(97)00307-1.
- [63] J.-N. Chazalviel, M. Etman, F. Ozanam, A voltammetric study of the anodic dissolution of p-Si in fluoride electrolytes, *J. Electroanal. Chem. Interfacial Electrochem* 297 (1991) 533–540, doi:10.1016/0022-0728(91)80049-V.
- [64] S. Menezes, B. Miller, K.J. Bachmann, Electrodeposition and passivation phenomena in III-V semiconducting compounds, *J. Vac. Sci. Technol. B Microelectron. Process. Phenom.* 1 (1983) 48–53, doi:10.1116/1.582541.
- [65] H.H. Goossens, W.P. Gomes, (Photo)electrochemistry: a suitable tool for investigating wet etching processes on III-V semiconductors, *Electrochim. Acta* 37 (1992) 811–826, doi:10.1016/0013-4686(92)85034-1.